Published in final edited form as:
Science. 2017 June 30; 356(6345): 1379–1383. doi:10.1126/science.aam5887.

Decoding of position in the developing neural tube from antiparallel morphogen gradients

Marcin Zagorski[1], **Yoji Tabata**[2], **Nathalie Brandenberg**[2], **Matthias Lutolf**[2], **Gašper Tkačik**[1], **Tobias Bollenbach**[1,3,*], **James Briscoe**[4,*], and **Anna Kicheva**[1,4,*]

[1]Institute of Science and Technology IST Austria, 3400 Klosterneuburg, Austria [2]Institute of Bioengineering, School of Life Sciences (SV) and School of Engineering (STI), Ecole Polytechnique Fédérale de Lausanne (EPFL), Lausanne, Switzerland [3]Institute for theoretical Physics, University of Cologne, Germany [4]The Francis Crick Institute, 1 Midland Road, NW1 1AT, London, UK

Abstract

Like many developing tissues, the vertebrate neural tube is patterned by antiparallel morphogen gradients. To understand how these inputs are interpreted, we measured morphogen signaling and target gene expression in mouse embryos and chick ex vivo assays. From these data, we derived and validated a characteristic decoding map that relates morphogen input to the positional identity of neural progenitors. Analysis of the observed responses indicates that the underlying interpretation strategy minimizes patterning errors in response to the joint input of noisy opposing gradients. We reverse-engineer a transcriptional network that provides a mechanistic basis for the observed cell fate decisions and accounts for the precision and dynamics of pattern formation. Together, our data link opposing gradient dynamics in a growing tissue to precise pattern formation.

In the developing vertebrate neural tube, Sonic hedgehog (Shh) and Bone morphogenetic proteins (BMP) form antiparallel signaling gradients along the dorsoventral (DV) axis ((1, 2), Fig. 1A). Neural progenitors along the entire axis can respond to both Shh and BMP signaling (3, 4). Antiparallel gradients can theoretically provide more precise positional information than single gradients (5–7) raising the possibility that the precise DV pattern of neural progenitor identities depends on the integration of Shh and BMP signals.

To test this, we first measured the BMP and Shh signaling profiles in the growing mouse neural tube (Fig. 1A-D, Fig. S1, S2, Table S1), using phosphorylated Smad1/5/8 (pSmad) as BMP signaling readout and a transcriptional reporter for Shh signaling (GBS-GFP) (8, 9). The levels of Shh and BMP signaling as a function of the absolute distance to the source did not change appreciably during the first 30h of development (Fig. 1B, C). At later times, the gradient amplitudes decreased (Fig. 1B, C). Hence, the two signaling gradients had their greatest range at the earliest developmental stages. Subsequently, as the tissue increased in size (9), the relative ranges of the gradients decreased (Fig. 1D, Fig. S2B).

*Correspondence to: anna.kicheva@ist.ac.at, james.briscoe@crick.ac.uk, t.bollenbach@uni-koeln.de.

Europe PMC Funders Author Manuscripts

For the signaling gradients to accurately specify positional identities along the entire DV axis, they have to contain sufficiently precise positional information. To test this, we quantified their positional error (10, 11). For each gradient, the positional error is approximately one cell diameter close to the respective morphogen source but increases away from the source (Fig. 1E). Neither the Shh, nor the BMP signaling gradient alone provides precise positional information throughout the DV axis. By contrast, the joint positional error (7, 10) resulting from the combined interpretation of both signals is <3 cell diameters at 5h and approximately uniform across the DV axis prior to 30h of development (Fig. 1E, Fig. S2C). After 30h, the Shh and BMP signaling levels markedly decrease in the middle of the DV axis and the positional error increases to >20 cell diameters (Fig. 1E). Thus, together the Shh and BMP gradients can provide precise positional information along the entire DV axis prior to ~30h.

To assess the precision of pattern, we measured the expression profiles of Nkx6.1 and Pax3. These transcription factors are expressed in distinct progenitor domains (Fig. 1F, Fig. S2A) and are part of the morphogen-driven gene regulatory network that controls neuronal subtype specification (2). Prior to 30h, Nkx6.1 and Pax3 had graded profiles that correlated with Shh and BMP signaling profiles, respectively (Pearson's correlation coefficients 0.9, Fig. S2D-F). After 30h, Nkx6.1 and Pax3 expression became step-like and the correlation was lost (Fig. S2F). The standard deviations of the Nkx6.1 and Pax3 boundary positions (Fig. S2G, H) after 50h were ≤3 cell diameters, whereas the positional error of the signaling gradients was >10 cell diameters (Fig. 1E). This suggests that the gene expression domains are established at early developmental times and then become independent of morphogen signaling after 30h (9).

The similarity in the precision of signaling profiles at early times (Fig. 1E) and target gene boundary positions (Fig. S2H) suggested that cells interpret the signals in a way that minimizes pattern imprecision. Theoretical studies (7, 12) have shown that a decoding strategy that ensures minimum positional imprecision given noisy gradients is maximum-likelihood (ML) estimation of position from the joint morphogen signaling levels (10). ML estimation uses the observed mean and variance of a set of signaling profiles to determine the probability distributions of positional identities that correspond to any given combination of Shh and BMP signaling ((10), eq. 1). The maxima of these probability distributions represent a ML decoding map. Thus, if the interpretation mechanism in the neural tube represents an optimal decoding strategy that minimizes imprecision, then the positional identities adopted for arbitrary combinations of Shh/BMP signaling would be the same as predicted by ML estimation. To test this, we used the observed signaling profiles at 5h to calculate the distributions of positional identities for any combination of Shh/BMP signaling (Fig. S3, (10)) and determined the ML decoding map (Fig. 2A).

Inspection of the map suggested that the pattern would shift for signaling profiles different from wildtype. Shh-GFP homozygous embryos (Shh^{Hypo}) are hypomorphic for Shh signaling (13) (Fig. S4). In these embryos, the amplitudes of the signaling profiles and the absolute pSmad decay length were similar to wildtype for most time points (Fig. 2B, C, Fig. S5). However, the decay length of the Shh signaling gradient was smaller than wildtype in absolute units and relative to tissue size (t-test p-value<0.005, Fig. 2B, Fig. S5B). Hence, at

5h of development the levels of Shh/BMP along the DV axis in the Shh^{Hypo} differed from wildtype (Fig. 2A). In the ML decoding map, equivalent positions along the DV axis of Shh^{Hypo} and wildtype are associated with different positional identities (Fig. 2A, D). These predicted shifts are consistent with the experimentally observed ventral shifts of the Nkx6.1 and Pax3 boundaries in Shh^{Hypo} compared to wildtype (Fig. 2D).

A noteable feature of the ML decoding map is that intermediate identities are obtained only for low levels of both morphogens (Fig. 2A, Fig. S3A). At high levels of both signals, unlike the unimodal distributions of positional identities obtained at most Shh/BMP combinations, the distributions are bimodal, with low probability of adopting intermediate identities (Fig. S3B). To test this, we measured the response of chick neural plate [i]-explants to defined concentrations of Shh and BMP7 after 24h of culture (Fig. 3A-C, Fig. S6, (10)). We assayed expression of target genes that subdivide the DV axis into distinct domains (Fig. 3A, Fig. S6A). Consistent with previous results (14), in the absence of BMP, addition of 1nM Shh resulted in explants expressing predominantly Olig2, whereas Nkx2.2 was expressed in most cells exposed to 4nM Shh (Fig. 3B, C). In response to low or no Shh, explants acquired dorsal Pax7+ fates (3). Low levels of both Shh and BMP (0.5nM Shh, 0.05nM BMP) resulted in explants adopting an intermediate identity, marked by expression of genes such as Dbx1 and Nkx6.1 (Fig. S6), but not Pax7, Olig2 or Nkx2.2 (Fig. 3B, C).

Exposure to high concentrations of both Shh and BMP resulted in a different outcome. Explants treated with 2-4nM Shh and 0.5-1nM BMP contained a mixture of cells with dorsal (Pax7+) and ventral identities (Nkx2.2+ or Olig2+) (Fig. 3B, C), but no Dbx1+ intermediate identities (Fig. S6, Table S2). Dorsal and ventral markers were not co-expressed in the same cell, but were observed in adjacent cells (Fig. 3C), indicating that individual cells make a definitive decision between ventral or dorsal identities. We validated these responses using a novel microfluidic device that allows us to culture explants in defined antiparallel gradients ((10), Fig. S7, S8). A region of intermediate identities was apparent at low Shh/BMP concentrations (~0.05nM Shh, ~0.02nM BMP7), while intermixed or directly adjacent Pax7+ and Olig2+ cells occurred at high concentrations (Fig. 3D). Thus, the ML decoding map captures the experimentally observed distinct responses to low and high signaling levels of both morphogens and provides a characteristic signature of a strategy that minimizes the imprecision of pattern. This rules out mechanisms such as interpretation of the difference or the ratio of the two signals (e.g. (15)), which would generate similar responses at low and high levels of signaling (Fig. S9).

The decoding map is a phenomenological model of patterning that does not describe a specific molecular mechanism. Thus, the question remains as to how the observed decoding strategy is molecularly implemented. We hypothesized that the observed responses can be explained by the dynamics of the morphogen-controlled transcriptional network in the neural tube. To test this, we extracted a core network for the central region of the neural tube (Fig. 4A). This region expresses Dbx1/2, adjacent to the Nkx6.1/6.2 domain ventrally, and the Pax3/7 domain dorsally (16–18). Cross-repressive interactions between pairs of these genes have been identified (16–20). We therefore conceived a network composed of dorsal (D; e.g. Pax3), intermediate (I; e.g. Dbx2) and ventral (V; e.g. Nkx6.1) transcription factors and used this as the basis of a computational screen (21) for networks that would reproduce

the experimental observations (Fig. 4B, (10)). Using the measured signaling profiles as input (Fig. 1D), we obtained 1221 parameter sets, from 600 million randomly sampled, that recapitulated the key experimental observations and reproduced the characteristic decoding map. Principal component analysis did not reveal distinct clusters (Fig. 4C) and for 99.6% of the sets, interpolating parameter values between at least two sets resulted in solutions that passed the screening criteria. This suggested a connected parameter subspace. Many of the successful solutions had three stable fixed points (34%), were insensitive to initial conditions, and matched the measured precision of target gene boundaries (Fig. S10).

The successful solutions displayed common features. The activation of I by morphogen signaling was weaker than the activation of V by Shh and D by BMP (Fig. 4D) and was not required (Table S3). The width of the I stripe correlated negatively with the strength of I repression by D and V, and the strength of D and V activation by morphogens (Fig. S10C). Thus, high levels of signaling induce V and D fates, which in turn repress the I fate. The specification of intermediate identities requires the levels of signaling of *both* morphogens to be low, explaining how the transcriptional network produces the signature of the ML decoding map. All repressive cross-interactions were required (Table S3) and tightly constrained (Fig. 4D, Fig. S10D). Cross-repressive interactions generate multistability of gene expression and this could explain how pattern is maintained independent of morphogen signaling at later times. Simulating the network dynamics with signaling input restricted to progressively shorter periods revealed that signaling is essential only during the first 15h (Fig. S10E).

Finally, the network model also predicted the effect of genetic perturbations that were not part of the screening criteria. Shh null mutants lack ventral and most intermediate identities (22, 23), whereas embryos lacking Shh and Gli3, the main Gli repressor, recover some ventral cell types and express Nkx6.1 (23, 24). Simulations of the VID network were consistent with these observations (Fig. S11).

Transcriptional networks are versatile (25) and can support robust information processing (26). In the mouse neural tube, we uncovered a transcriptional network that allows neural progenitors to integrate information from the opposing gradients. The resulting response has the characteristics of a decoding strategy that maximizes the precision of pattern (Fig. S12). Thus, the regulatory network integrates two graded inputs to precisely measure location in a developing tissue and maintains accurate pattern as the tissue grows.

Supplementary Material

Refer to Web version on PubMed Central for supplementary material.

Acknowledgments

We thank T. Jessell and E. Laufer for antibodies. Funding: IST Austria (MZ, GT, TB, AK); Austrian Science Fund (FWF P 28844) (GT); European Research Council under European Union's Horizon 2020 research and innovation programme (680037) (MZ, AK); People Programme (Marie Curie) of the European Union's Seventh Framework Programme, REA 291734 (MZ); the Francis Crick Institute which receives its core funding from Cancer Research UK (FC001051), UK Medical Research Council (FC001051), Wellcome Trust (FC001051 and WT098326MA) (JB, AK); ERC grant (StG_311422) and the EU framework 7 HEALTH research programme PluriMes (http://www.plurimes.eu/) (YT, NB, ML). Supplement contains additional data.

References and Notes

1. Briscoe J, Small S. Morphogen rules: design principles of gradient-mediated embryo patterning. Development. 2015; 142:3996–4009. [PubMed: 26628090]
2. Alaynick WA, Jessell TM, Pfaff SL. SnapShot: Spinal Cord Development. Cell. 2011; 46:178.
3. Liem KF, Jessell TM, Briscoe J. Regulation of the neural patterning activity of sonic hedgehog by secreted BMP inhibitors expressed by notochord and somites. Development. 2000; 127:4855–66. [PubMed: 11044400]
4. Mizutani CM, Meyer N, Roelink H, Bier E. Threshold-dependent BMP-mediated repression: A model for a conserved mechanism that patterns the neuroectoderm. PLoS Biol. 2006; 4:1777–1788.
5. Morishita Y, Iwasa Y. Accuracy of positional information provided by multiple morphogen gradients with correlated noise. Phys Rev E. 2009; 79:61905.
6. Dubuis JO, Tkačik G, Wieschaus EF, Gregor T, Bialek W. Positional information, in bits. Proc Natl Acad Sci U S A. 2013; 110:16301–8. [PubMed: 24089448]
7. Tkačik G, Dubuis JO, Petkova MD, Gregor T. Positional information, positional error, and readout precision in morphogenesis: a mathematical framework. Genetics. 2015; 199:39–59. [PubMed: 25361898]
8. Balaskas N, et al. Gene regulatory logic for reading the Sonic Hedgehog signaling gradient in the vertebrate neural tube. Cell. 2012; 148:273–84. [PubMed: 22265416]
9. Kicheva A, et al. Coordination of progenitor specification and growth in mouse and chick spinal cord. Science. 2014; 345:1254927. [PubMed: 25258086]
10. See Supplementary materials.
11. Bollenbach T, et al. Precision of the Dpp gradient. Development. 2008; 135:1137–1146. [PubMed: 18296653]
12. Morishita Y, Iwasa Y. Coding design of positional information for robust morphogenesis. Biophys J. 2011; 101:2324–2335. [PubMed: 22098730]
13. Chamberlain CE, Jeong J, Guo C, Allen BL, McMahon AP. Notochord-derived Shh concentrates in close association with the apically positioned basal body in neural target cells and forms a dynamic gradient during neural patterning. Development. 2008; 135:1097–106. [PubMed: 18272593]
14. Dessaud E, et al. Interpretation of the sonic hedgehog morphogen gradient by a temporal adaptation mechanism. Nature. 2007; 450:717–20. [PubMed: 18046410]
15. McHale P, Rappel W-J, Levine H. Embryonic pattern scaling achieved by oppositely directed morphogen gradients. Phys Biol. 2006; 3:107–20. [PubMed: 16829697]
16. Briscoe J, Pierani a, Jessell TM, Ericson J. A homeodomain protein code specifies progenitor cell identity and neuronal fate in the ventral neural tube. Cell. 2000; 101:435–45. [PubMed: 10830170]
17. Moore S, et al. Distinct regulatory mechanisms act to establish and maintain Pax3 expression in the developing neural tube. PLoS Genet. 2013; 9:e1003811. [PubMed: 24098141]
18. Vallstedt A, et al. Different levels of repressor activity assign redundant and specific roles to Nkx6 genes in motor neuron and interneuron specification. Neuron. 2001; 31:743–55. [PubMed: 11567614]
19. Sander M, et al. Ventral neural patterning by Nkx homeobox genes : Nkx6.1 controls somatic motor neuron and ventral interneuron fates. Genes Dev. 2000; 14:2134–2139. [PubMed: 10970877]
20. Oosterveen T, et al. Mechanistic differences in the transcriptional interpretation of local and long-range Shh morphogen signaling. Dev Cell. 2012; 23:1006–1019. [PubMed: 23153497]
21. Ben-zvi D, Shilo B, Fainsod A, Barkai N. Scaling of the BMP activation gradient in Xenopus embryos. Nature. 2008; 453:1205–11. [PubMed: 18580943]
22. Chiang C, et al. Cyclopia and defective axial patterning in mice lacking Sonic hedgehog gene function. Nature. 1996; 383:407–413. [PubMed: 8837770]
23. Litingtung Y, Chiang C. Specification of ventral neuron types is mediated by an antagonistic interaction between Shh and Gli3. Nat Neurosci. 2000; 3:979–85. [PubMed: 11017169]

24. Persson M, et al. Dorsal-ventral patterning of the spinal cord requires Gli3 transcriptional repressor activity. Genes Dev. 2002; 16:2865–78. [PubMed: 12435629]
25. Cotterell J, Sharpe J. An atlas of gene regulatory networks reveals multiple three-gene mechanisms for interpreting morphogen gradients. Mol Syst Biol. 2010; 6:1–14.
26. Tkačik G, Bialek W. Information Processing in biological systems. Annu Rev Cond Matt Phys. 2016; 7:89–117.

Europe PMC Funders Author Manuscripts

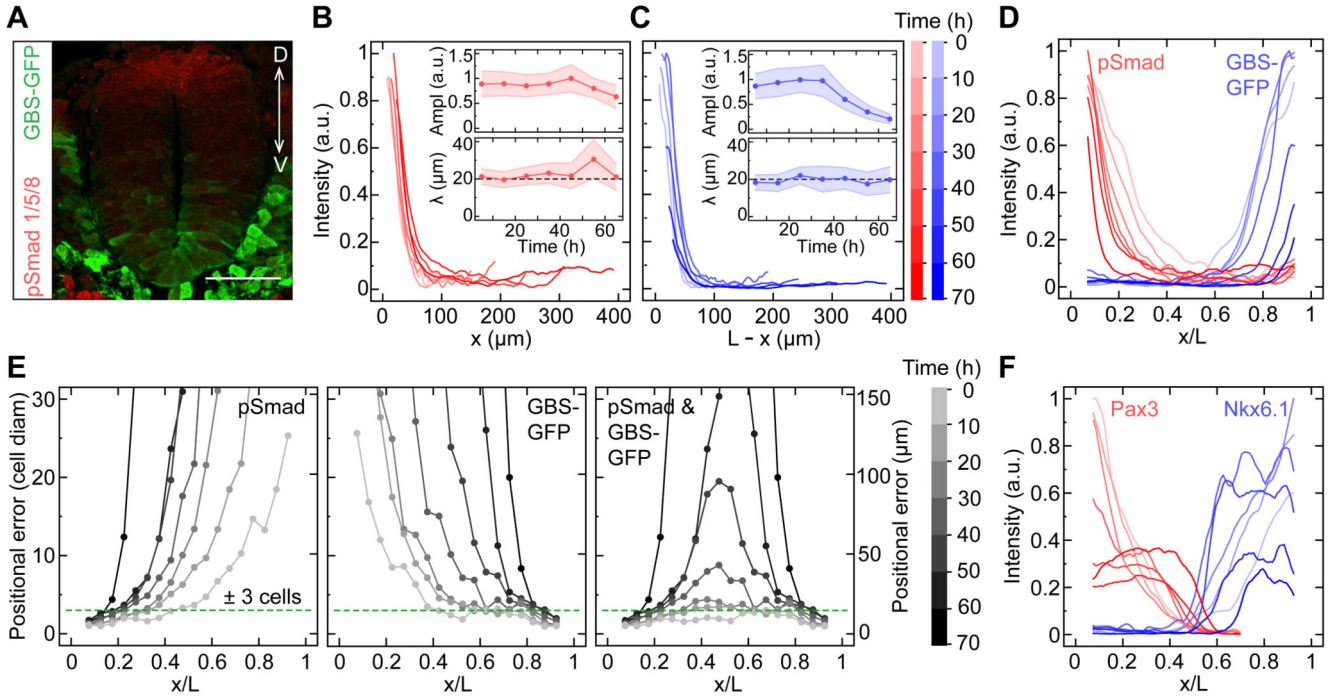

Figure 1.

A) Brachial cross-section of mouse neural tube at 30h, immunostained for GBS-GFP and pSmad1/5/8. Scale bar, 50μm. **B, C)** Mean pSmad (B) and GBS-GFP (C) profiles at different developmental stages (sample sizes, Table S1). **D)** Mean pSmad and GBS-GFP profiles as a function of relative DV position. Time color-code in C. **E)** Positional error of pSmad and GBS-GFP gradients. Joint positional error of pSmad and GBS-GFP (last panel). **F)** Mean Pax3 and Nkx6.1 expression profiles. Time color-code in C.

Europe PMC Funders Author Manuscripts

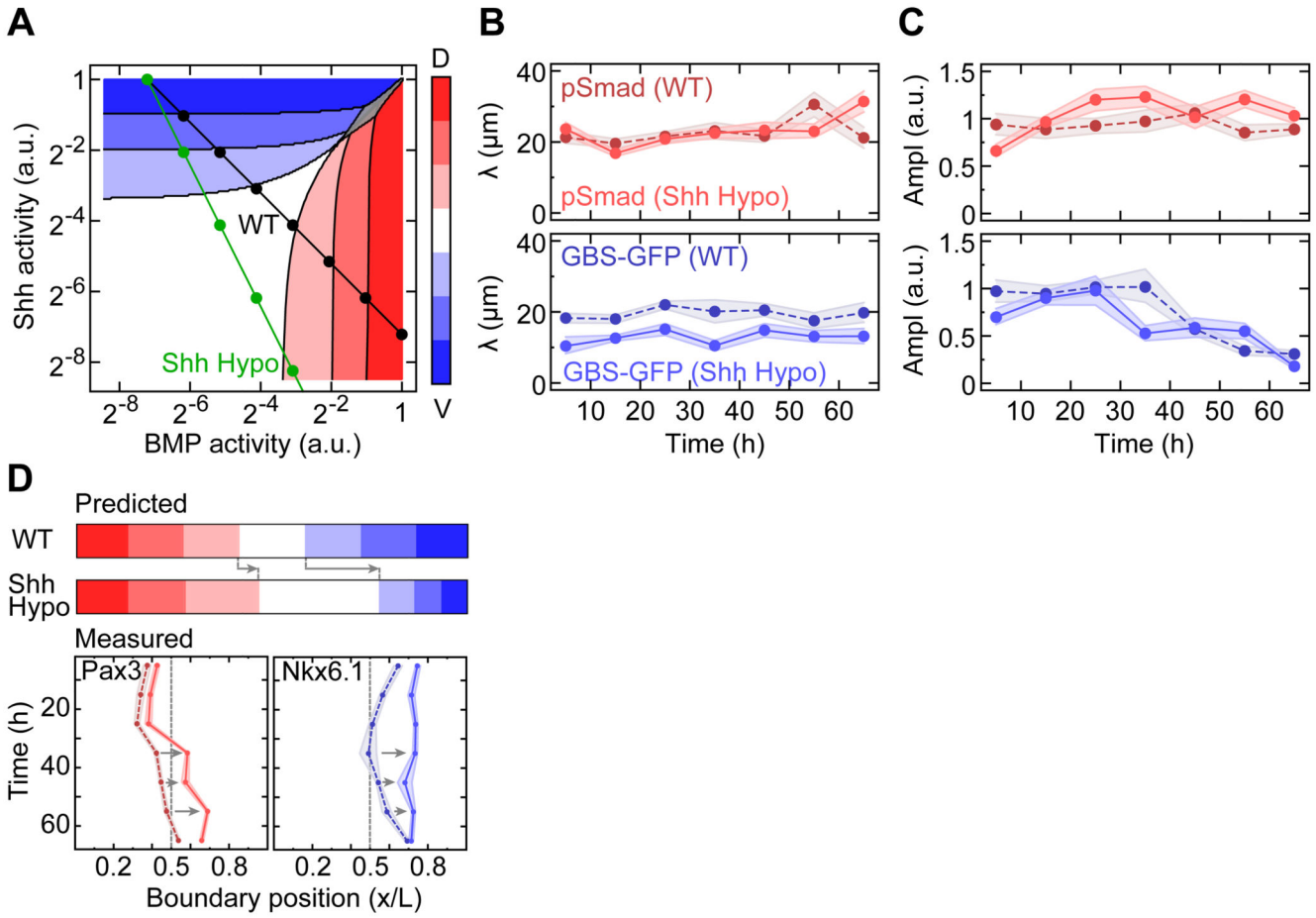

Figure 2.

A) ML decoding map obtained from wildtype mouse sections at 5h, using a parameter-free procedure (eq. 1, (10)). Colors correspond to predicted positional identities. Mean pSmad and GBS-GFP levels from exponential fits to the profiles, black line (wildtype), green (Shh^{Hypo}). Dots, 7 equidistant positions along DV axis. In Shh^{Hypo} the GBS-GFP profile decay length is half of WT. The probability distributions of DV identities are bimodal in the grey region. **B)** Exponential decay lengths of pSmad and GBS-GFP for Shh^{Hypo} (solid) and wildtype (dashed) datasets. Shaded regions, 95% CI from bootstrapping. **C)** Amplitudes of pSmad and GBS-GFP profiles, denoted as in B. **D)** Above: DV identities predicted from the decoding map in A. Below: measured Pax3 and Nkx6.1 boundary positions in Shh^{Hypo} (solid) are shifted ventrally compared to wildtype (dashed).

Europe PMC Funders Author Manuscripts

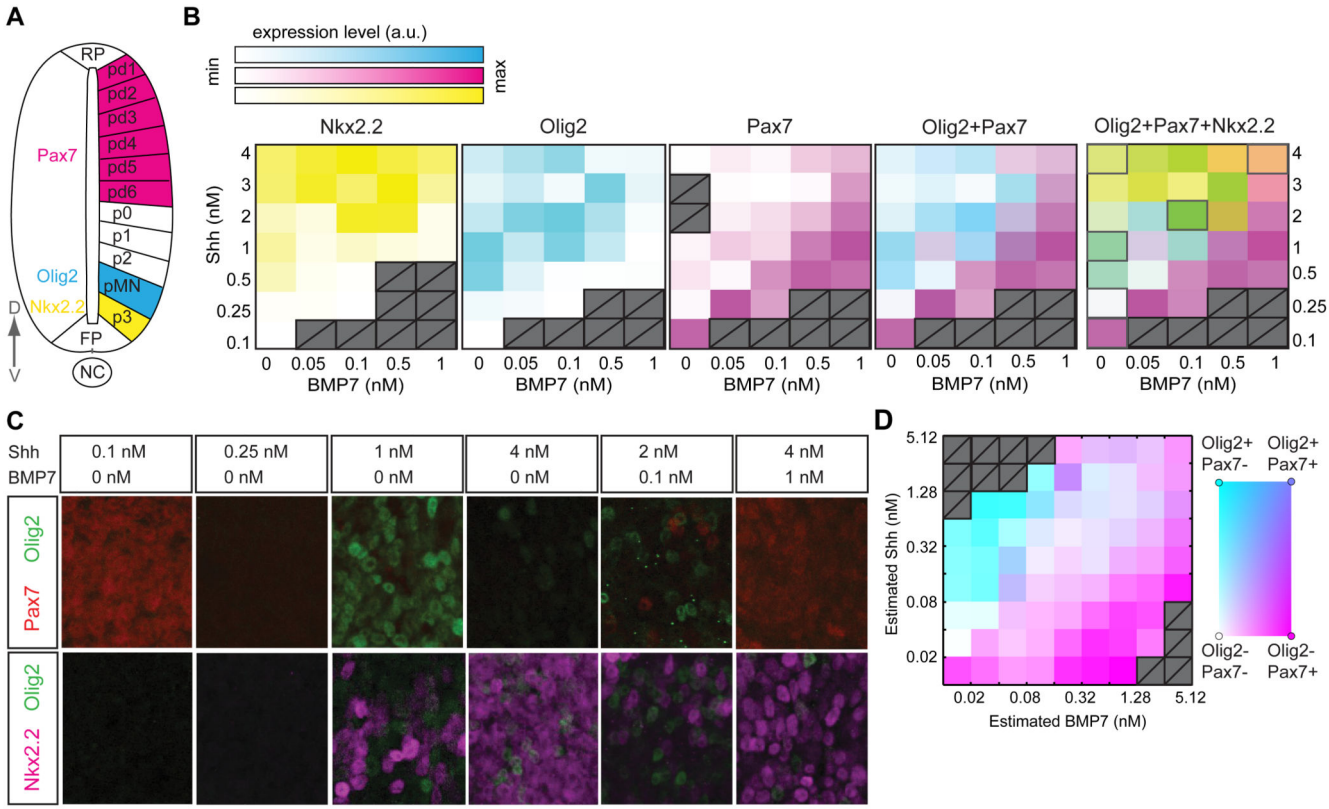

Figure 3.

A) DV expression domains of indicated genes (see also (2)). **B)** Mean proportion of explant area positive for Pax7 (magenta), Olig2 (cyan) or Nkx2.2 (yellow) after culture in the indicated Shh and BMP7 concentrations for 24h (sample sizes, Table S2). Last panels are overlays. **C)** Representative images for the conditions outlined in grey in the last panel of B. **D)** Proportion of Pax7 and Olig2 positive pixels as a function of the calibrated Shh/BMP7 concentrations for a set of explants cultured in microfluidic devices. Color legend (right). Sample size, mean per bin n=4.7 (min. 2, max. 14). Hatched regions, not sampled.

Europe PMC Funders Author Manuscripts

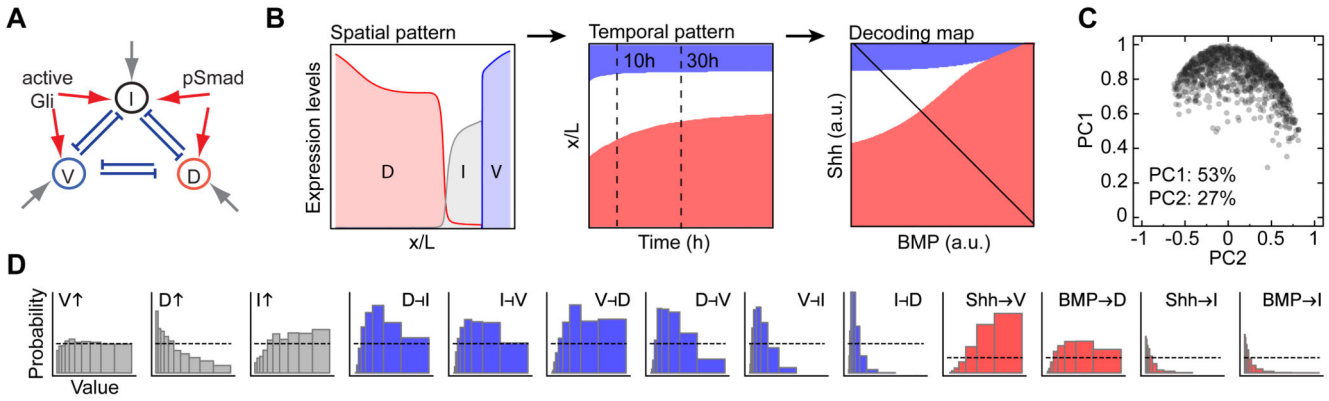

Figure 4.

A) Morphogen-driven transcriptional network in the neural tube. Shh and BMP signaling activate ventral (V), intermediate (I) and dorsal (D) target TFs. Uniform activating inputs (grey arrows). Degradation not depicted. **B)** Criteria of the computational screen. **C)** Principal component analysis of successful parameter sets. Contributions of the first two principal components to the total variation indicated. **D)** Distribution of parameter values for solutions that pass the screen. Uniform random distributions (dashed lines) are given for comparison.

Europe PMC Funders Author Manuscripts